Realization of Smooth Pursuit for a Quantized Compliant Camera Positioning System

Michael D. Kim and Jun Ueda

***Abstract*—This paper presents a discrete switching controller for a realization of smooth pursuit. The human eye can produce both rapid and smooth movements, positioned by muscles that are a collection of quantized flexible motor units. From a control point of view, smooth pursuit can be considered as velocity matching control of an impulsive dynamical system. This may be feasible by a conventional pulsewidth modulation (PWM) controller; however, it causes high-frequency switching in each motor unit and may damage a compliant actuation system. The proposed controller generates reduced switching by optimizing a series of discrete switching commands at each primitive in an open-loop manner. This study uses a camera positioner driven by quantized compliant actuators and aims to match the velocity of a target object, while images are being captured to avoid motion blur. After images are obtained, the discrete switching controller suppresses residual vibrations to reduce switching further. Experimental results demonstrate that the proposed discrete switching controller outperformed the classical PWM controller and successfully tracked an object of interest during an exposure window.**

***Index Terms*—Compliant, quantized, robot vision, smooth pursuit, vibration.**

I. Introduction

Compliant actuators have been widely studied in recent years to mimic biological systems. One of the interest systems has been the human ocular system that has two representative movements: saccade and smooth pursuit. The saccade is an accurate rapid point-to-point motion whose settling time is 50 ms and velocity is known to be 250–500 °/s [1]. Smooth pursuit is the key component for tracking, which allows the eyes to follow a moving object of interest [2].

Inspired by these observations, there have been various efforts in the robotic eye system. Camera positioning systems driven by compliant mechanisms have been proposed [3], [4] and focused on the generation of saccade-like movements. There have also been studies that focused on smooth pursuit and object detection using humanoid vision systems [5]–[7] and robotic eyes [8], [9] actuated by conventional servo motors. However, the quantization effect in the actuation system was not taken into account although existing studies have shown notable results.

A physiological study has reported that the human ocular system is controlled by impulsive inputs [10]. In addition, motor units in the biological system, muscle fibers, are operated in an ON–OFF manner [11]. These physiological pieces of evidence indicate that open-loop quantized controllers that switch the binary states in motor units are utilized to generate movements. Such velocity control is fairly easy when an electromagnetic servomotor is used. However, this is not the case in the neuromotor system primarily due to recruitment [10]. Muscles are essentially quantized actuators that cannot produce continuous force. Despite quantized force production, we are not aware of this discrete actuation in the eye and able to perceive the features of a moving object. Although possible neuromotor mechanisms in smooth pursuit are debatable, from an engineering point of view, this problem can be seen as velocity matching control of an impulsive dynamical system.

This paper presents a realization of smooth pursuit for a quantized compliant actuation system. Fig. 1(a) shows a robotic vision system developed by the authors' group [12]. The design was inspired by the biological system that a camera was driven by an antagonistic pair of cellular actuators. The cellular actuator exhibits quantization and compliance. Saccade-like movements have been investigated in the authors' previous works [13]–[15], and thus, this study focuses on smooth pursuit. The initial concept of this work has been presented in [16]. This paper includes refinement of the proposed method, performance metrics, and additional experimental results.

The proposed controller is designed to generate velocity profiles for tracking an object of interest only during exposure windows of a camera. Additionally, discrete switching commands are generated to sup-

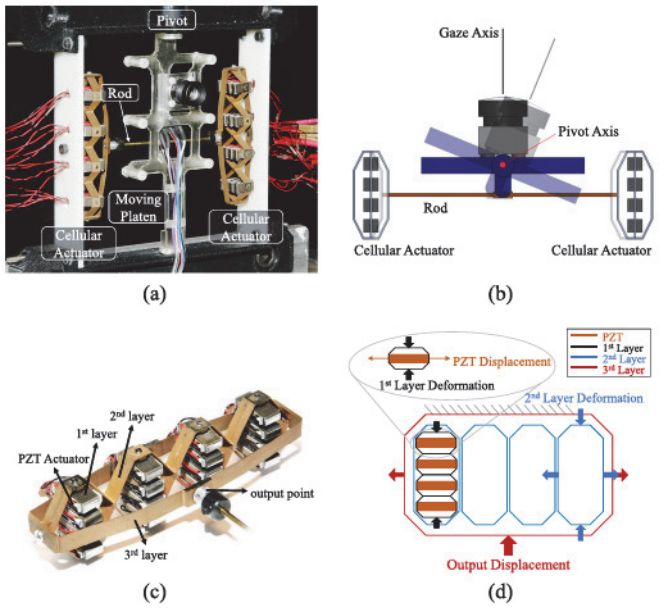

Fig. 1. Robotic vision system. (a) One-degree-of-freedom motion generated by an antagonistic pair actuators. (b) Pictorial representation of the camera positioning system. (c) Cellular actuator. (d) Pictorial representation of the cellular actuator.

Manuscript received January 27, 2018; accepted May 20, 2018. Date of publication August 8, 2018; date of current version October 2, 2018. This paper was recommended for publication by Associate Editor A. Ude and Editor T. Murphey upon evaluation of the reviewers' comments. This work was supported by the National Science Foundation under Dynamical Systems Grant CMMI-1300019 and Grant CMMI-1662029. The work of M. D. Kim was supported in part by the Georgia Tech Presidents Fellowship. *(Corresponding author: Michael D. Kim.)*

M. D. Kim was with the Bio-Robotics and Human Modeling Lab, George W. Woodruff School of Mechanical Engineering, Georgia Institute of Technology, Atlanta, GA 30332 USA. He is now with Sandia National Laboratories, Livermore, CA 94550 USA (e-mail: mkim44@gatech.edu).

J. Ueda is with the Bio-Robotics and Human Modeling Lab, George W. Woodruff School of Mechanical Engineering, Georgia Institute of Technology, Atlanta, GA 30332 USA (e-mail: jun.ueda@me.gatech.edu).

Color versions of one or more of the figures in this paper are available online at http://ieeexplore.ieee.org.

Digital Object Identifier 10.1109/TRO.2018.2858272

press residual vibrations after acquiring images, which could decrease the amount of switching. We consider that tracking the object of interest only when images are being obtained fulfills the function of smooth pursuit. The proposed method is validated by a direct comparison with the reference motion and by pseudotracking a slowly moving object.

II. Camera Positioning System

A. Mechanism

The robotic vision system is driven by the cellular actuator consisting of 16 piezoelectric (PZT) actuators, as shown in Fig. 1(c). When the PZT actuator is activated, a linear displacement is generated at the output point of the cellular actuator through the multilayer mechanism, as depicted in Fig. 1(d) [12]. This multilayer mechanism is made of brass and has a thickness of 170 μm, introducing compliance and enabling linear motion at the output point. Two cellular actuators are connected to a moving platen via a rod and placed in an antagonistic fashion. The rod and pivot axes are perpendicular, while a linear offset exists. Therefore, the camera experiences a rotational motion when the rod is positioned by the cellular actuators, as depicted in Fig. 1(b). A high ratio of the translation motion to the rotational motion is used to introduce quantization to the system and achieve a sufficient angular displacement of $\pm 10.3^\circ$. The resolution and travel range of the system can be determined by adjusting this ratio and the number of PZTs in the cellular actuator.

B. Cellular Actuator: Compliance and Quantization

In this study, each PZT actuator is independently operated in a quantized manner, as if each motor unit in the biological system is switched between contraction and relaxation. To activate or deactivate the PZT actuators, impulsive inputs are given to the system. Therefore, the cellular actuator is a quantized system. This approach is similar to biological muscular tissue in that the action is generated by the recruitment of individual PZT actuators activated. In a control perspective, the binary operation of motor units avoids hysteresis and nonlinearity in the PZT actuator [14]. In addition, the cellular actuator exhibits compliance, as aforementioned in Section II-A. The compliant mechanism enables rapid motion comparable to the ocular motion by amplifying displacement from the limited PZT stroke.

C. Dynamics

The camera positioning system was experimentally modeled by observation of step and shaped responses. It was observed that the poles are located at $-13.6 + j70.3$, $-13.6 - j70.3$, and -200 with no zeros. In this paper, the nondominant pole was neglected, and thus, the system was modeled as a second-order linear system. Assuming no external disturbances, the model of the camera positioning system driven by the quantized complaint cellular actuator can be represented as

$$G(s) = \frac{K}{s^2 + 2\zeta\omega_n s + \omega_n^2} \tag{1}$$

where K is the residue, ω_n is the natural frequency, and ζ is the damping coefficient. The value of ω_n, ζ, and K are 71.63 rad/s, 0.19, and 3288.3, respectively.

III. Quantization Effects

Due to independent binary operations in the individual units, the output displacements of the cellular actuator are discrete, as shown in Fig. 2(a). Consequently, the angular displacements of the camera positioning system with respect to the number of PZT actuators activated

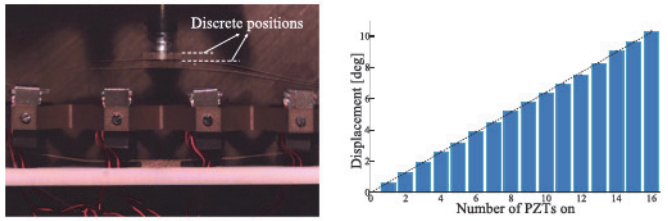

Fig. 2. Quantization effect. (a) Discrete output positions due to the binary operation. (b) Calibration.

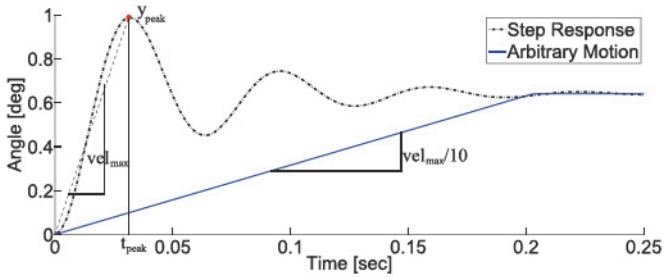

Fig. 3. Step response of the camera positioning system. This study is interested in generation of motion with the velocity slower than the early stage of the step response.

are discrete, as shown in Fig. 2(b). We observed a resolution of 0.6407° with the standard deviation of 0.0032° in the camera positioning system.

Let p_k be the activation level of the cellular actuator, and a total of k PZT actuators are activated. Then, the corresponding discrete output position θ_k is

$$\theta_k = z \cdot p_k \tag{2}$$

where z is a linear mapping observed in Fig. 2(b).

To reproduce smooth-pursuit-like movements, this study aims to generate an arbitrary velocity profile from a discrete position θ_k to the next discrete position θ_{k+1}. The motion $\mathbf{y}$ can be achieved by

$$\mathbf{y}(t) = f(\mathbf{x}(t),\, \mathbf{u}(t),\, t),\, y(0) = \theta_k \tag{3}$$

where t is the time, f is the dynamics of the camera positioning system, $\mathbf{x}$ is the state, and $\mathbf{u}$ is the control input.

In order to achieve an arbitrary velocity profile, appropriate $\mathbf{u}(t)$ needs to be determined. Due to quantization effects in the actuation system, the control input must be discretized, while control inputs of conventional systems are continuous. Therefore, $\mathbf{u}(t) \in \mathcal{Z}$ must be imposed.

Fig. 3 shows a response of the camera positioning system when a single PZT actuator is activated. Let the maximum velocity in the course of transient response be simply equivalent to $y_{\text{peak}}/t_{\text{peak}}$. For tracking a slowly moving object, this paper focuses on velocity profiles that are slower than $\text{vel}_{\max}$. We consider velocity profiles comparable to $\text{vel}_{\max}$ as saccades.

Assume that a desired motion has a constant velocity that is ten times slower than $\text{vel}_{\max}$, as shown in Fig. 3. A conventional controller with pulsewidth modulation (PWM) quantization can be used to generate a slowly moving profiles; however, high-frequency switching in the individual PZT actuators may be necessary due to quantization [16]. In practice, this is not desirable because it may potentially damage the complaint mechanism. In addition, this approach has little in common

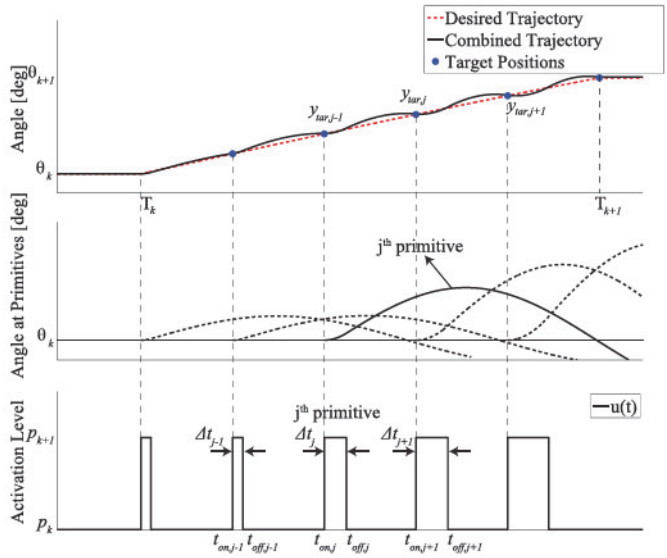

Fig. 4. Generation of discrete commands for velocity matching. The timings of primitive movements are determined to achieve the target positions indicated by blue circles at the time when the next primitive is generated.

with the actuation strategy in the biological system [17]. Therefore, a discrete switching controller should be developed.

IV. Commands for Smooth Pursuit

The proposed discrete switching controller is designed to track an object of interest only during the exposure windows. The discrete switching controller first generates commands to match the velocity of a target object, similar to smooth pursuit in the biological system. The commands are given to the system during the exposure windows, and thus, images can be obtained in the course of motion, while avoiding or mitigating blurriness of the object of interest. After images are obtained, additional discrete switching commands are generated for suppressing vibrations and reaching the desired position. The commands for vibration suppression require less switching than in the tracking period. No additional switching is required once the vibration is fully suppressed. Therefore, the second part limits switching in individual PZT units and avoids fatigue in the thin compliant mechanism.

A. Tracking Commands

The time response of the camera positioning system can be represented as

$$y(t) = \sum_{i=1}^{n} \frac{A_i \cdot 1(t-t_i)}{\omega_n^2}\left[1 - \frac{e^{-\zeta\omega_n(t-t_i)}}{\sqrt{1-\zeta^2}}\sin(\omega_d(t-t_i)+\psi)\right] + y_0, \quad A_i \in \mathcal{Z}\ \forall i \tag{4}$$

where y_0 is the initial position, n is the total number of inputs given to the system, $1(t)$ is the unit step function, A_i is the amplitude of the ith step input, t_i is the time of the given ith step input, ω_d is the damped natural frequency, and $\psi = \text{atan}(\frac{\sqrt{1-\zeta^2}}{\zeta})$.

The procedure of the proposed discrete switching controller is depicted in Fig. 4. A total of m pulses are given to the system to achieve the desired motion from the activation level p_k at time T_k to p_{k+1} at time T_{k+1}. There is a tradeoff between the number of pulses m and tracking performance. The number of pulses must be chosen to make the control frequency ω_c at least two times greater than the natural frequency ω_n to meet the Nyquist criterion.

Due to redundancies in the actuation system, a number of solutions exist. We reduce the solution space by generating the ON signal in a periodical manner

$$t_{\text{on},j} = T_k + \frac{T_{k+1}-T_k}{m}(j-1) \tag{5}$$

where j denotes the jth pulse. Some redundancy remains, so we narrow the solution space further by introducing the following constraints:

$$|A_{\text{on},j}| = |A_{\text{off},j}| = 1 \tag{6}$$

$$p_k \le \sum A_i \le p_{k+1} \quad \forall i. \tag{7}$$

This bounds the activation level between the start and desired discrete positions at any time, limiting the amplitude of residual oscillations in the compliant actuation system.

The desired profile $y_{\text{des}}(t)$ is divided into m target positions $y_{\text{tar},j}$ along the trajectory with a constant time interval as

$$y_{\text{tar},j} = y_{\text{des}}(t_{\text{on},j+1}). \tag{8}$$

At each primitive, a piecewise function consisting of ON and OFF step inputs is given to the system to satisfy (8) by adjusting Δt_j. Due to residual vibration, the time interval Δt_j is not simply linear with $y_{\text{tar},j}$ as in PWM. Timings of the OFF commands $t_{\text{off},j}$ are determined at each primitive in a recursive manner as follows.

Residual vibrations may exist in the system due to control inputs. Let the residual vibration at $t_{\text{on},j}$ be introduced into the system at $t_{r,j}$ with an amplitude of $A_{r,j}$ and a phase of $\phi_{r,j}$. Unlike A_i, the amplitude of the residual vibration $A_{r,j}$ is not necessarily an integer. After a pulse-like command is generated, three different signals, the residual vibration, and vibrations due to ON and OFF commands, can be represented as a single impulse response. Let $B_{r,j}$, $B_{\text{on},j}$, and $B_{\text{off},j}$ be the decayed amplitudes of the residual vibrations at time $t_{\text{off},j}$ due to $A_{r,j}$, $A_{\text{on},j}$, and $A_{\text{off},j}$, respectively:

$$B_{r,j} = A_{r,j} \cdot e^{-\zeta\omega_n(t_{\text{off},j}-t_{r,j})} \tag{9}$$

$$B_{\text{on},j} = -A_{\text{on},j} \cdot e^{-\zeta\omega_n(t_{\text{off},j}-t_{\text{on},j})} \tag{10}$$

$$B_{\text{off},j} = -A_{\text{off},j}. \tag{11}$$

Similarly, phases at time $t_{\text{off},j}$ can be determined as

$$\Phi_{r,j} = \omega_d(t_{\text{off},j} - t_{r,j}) + \phi_{r,j} \tag{12}$$

$$\Phi_{on,j} = \omega_d(t_{\text{off},j} - t_{\text{on},j}) + \psi \tag{13}$$

$$\Phi_{\text{off},j} = \psi \tag{14}$$

where $\Phi_{r,j}$, $\Phi_{\text{on},j}$, and $\Phi_{\text{off},j}$ are the phases of $B_{r,j}$, $B_{\text{on},j}$, and $B_{\text{off},j}$, respectively, at $t_{\text{off},j}$. An equivalent single impulse input with an amplitude of B_{eqv} and a phase of Φ_{eqv} given at time $t_{\text{off},j}$ representing these three signals can be determined as

$$B_{\text{eqv}} = \sqrt{(B1)^2 + (B2)^2} \tag{15}$$

$$\Phi_{\text{eqv}} = \text{atan}\left(\frac{B2}{B1}\right) \tag{16}$$

where

$$B1 = B_{r,j}\cos(\Phi_{r,j}) + B_{\text{on},j}\cos(\Phi_{\text{on},j}) + B_{\text{off},j}\cos(\Phi_{\text{off},j}) \tag{17}$$

$$B2 = B_{r,j}\sin(\Phi_{r,j}) + B_{\text{on},j}\sin(\Phi_{\text{on},j}) + B_{\text{off},j}\sin(\Phi_{\text{off},j}). \tag{18}$$

Therefore, after j pulse-like commands are given to the system, the response of the camera positioning system at time τ can be represented

as

$$y_j(\tau) = y_{\text{ref}} + z\left(\frac{B_{\text{eqv}}}{\omega_n^2\sqrt{1-\zeta^2}}e^{-\zeta\omega_n(\tau - t_{\text{off},j})} \times \sin(\omega_d(\tau - t_{\text{off},j}) + \Phi_{\text{eqv}})\right), \quad \tau > t_{\text{off},j} \tag{19}$$

where y_{ref} is the reference position to the desired motion, which is initially θ_k.

Timings of primitive movements are determined to achieve target positions at the time when the next primitive is generated. Therefore, timing of the OFF command can be determined by solving (19) for $t_{\text{off},j}$ while setting $\tau = t_{\text{on},j+1}$ and $y_j = y_{\text{tar},j}$. Since the pulse-like commands are generated at each primitive, the solution must satisfy

$$t_{\text{off},j} \in [t_{\text{on},j},\, t_{\text{on},j+1}]. \tag{20}$$

Therefore, $t_{\text{off},j}$ can be numerically determined by using bracketing methods [18], guaranteeing convergence. The following target positions can be achieved by substituting $A_{r,j+1}$, $\phi_{r,j+1}$, and $t_{r,j+1}$ with B_{eqv}, Φ_{eqv}, and $t_{\text{off},j}$, respectively, and repeating (9)–(20) from $j = 1$ to $j = m$.

B. Changing the Base Position

Due to the nature of pulse-like commands, the response settles back to the base position y_{base} after the target position is achieved at each primitive. In addition, the amplitude of the residual vibration B_{eqv} increases as the target position $y_{\text{tar},j}$ gets closer to the desired discrete position θ_{k+1}.

To avoid this issue, we change the base position y_{base} to θ_{k+1} when $y_{\text{tar},j}$ exceeds the midpoint $\frac{\theta_k + \theta_{k+1}}{2}$, or vice versa. In this case, the ON command is omitted and does not obey (5). After the base position is changed, the calculation of command timings is identical except the signs of succeeding A_js are inverted. The same procedures (9)–(20) are used to determine the succeeding $t_{\text{off},j}$.

Fig. 5(a) depicts the concept of changing the base position when the target position crosses the midpoint. It can be considered as the discrete switching controller is pushing the actuation system toward the midpoint by inducing the residual vibrations until the base position y_{base} is changed. Then, the discrete switching controller is gradually diminishing the residual vibrations to settle the actuation system at the desired discrete position θ_{k+1}.

By changing the base position, the amplitude of the residual vibration B_{eqv} can be reduced, and the range is approximately $[0, \frac{|A_i|}{2}]$; however, the range of B_{eqv} is approximately $[0, |A_i|]$ if the base position remains unchanged. This can be observed from Fig. 5(b) showing comparisons in the amplitude of the residual vibration between with and without changing the reference position. At each primitive, the discrete controller compensates for the discrepancy between the position due to a total of $j-1$ pulse-like commands and target position $y_{\text{tar},j}$. This discrepancy can be expressed as $|y_{\text{ref}} - y_{\text{tar},j}| - y_{j-1}(t_{\text{on},j+1})$, and the maximum displacement that the controller can generate at each primitive is $\Delta y_{\max} = y(\Delta t_{\text{on}})$. Therefore, changing the base position also helps to avoid possible failure of the controller due to excessive position discrepancy.

The program containing the proposed discrete switching controller is summarized by the pseudocode in Algorithm 1. Fig. 6 shows a simulation result of the proposed controller when tracking an arbitrary motion ($\text{vel}_{\max}/10$) presented in Fig. 3. Although minor position errors exist, it can be observed that the proposed controller successfully achieved the desired motion at low control frequency.

Algorithm 1: Discrete Controller for Tracking.

```
Input: desired motion y_des(t); number of pulses m;
Define timings of ON commands t_on,j by (5)
Define target positions y_tar,j by (6)
for each primitive j do
    if y_des,j−1 → y_des,j crosses the midpoint then
        Change the base position y_base
        Omit On command and ignore (5)
        Invert the signs of succeeding A_j s
Determine timings of OFF commands t_off,j
by (9)–(20)
Update residual vibrations:
B_r,j+1 = B_eqv, φ_r,j+1 = Φ_eqv, and t_r,j+1 = t_off,j
Output: Discrete switching input u(t)
```

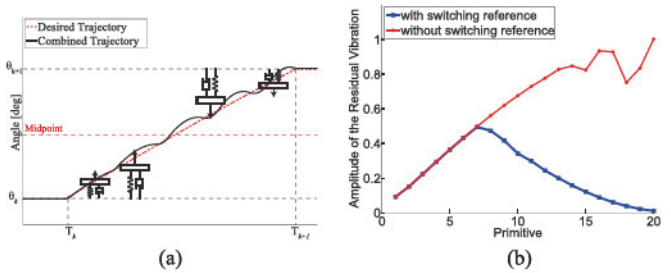

Fig. 5. (a) Conceptual depiction of the change in the base position when the desired motion crosses the midpoint. (b) Amplitude of the residual vibrations as the camera positioning system reaches to the desired position. Comparison between with and without changing the base.

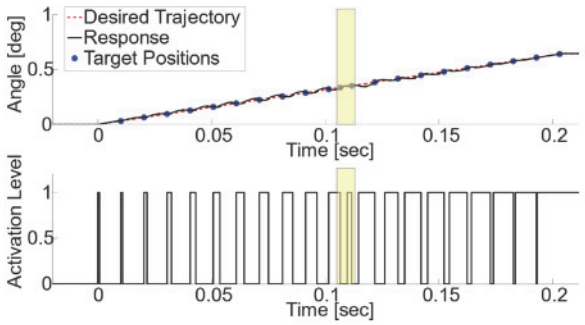

Fig. 6. Discrete switching commands for generating an arbitrary movement. The base position is changed in the highlighted region.

C. Vibration Suppression Commands

The proposed method is designed to match the velocity of the object of interest only during the exposure window, unlike other visual tracking methods for feeding video. We consider that acquisition of few images in one PZT increment is sufficient, since the field of view of the camera is not significantly changed. After the robotic vision system obtains images, the tracking commands are no longer necessary. Therefore, we suppress residual vibrations in the flexible system, while the camera positioning system reaches the desired quantized position. By this approach, switching can be further reduced, which prevents fatigue in the thin-layered mechanism. In order to achieve vibration suppression, the real and imaginary components of the residual vibrations must be zero. Therefore, a set of vibration

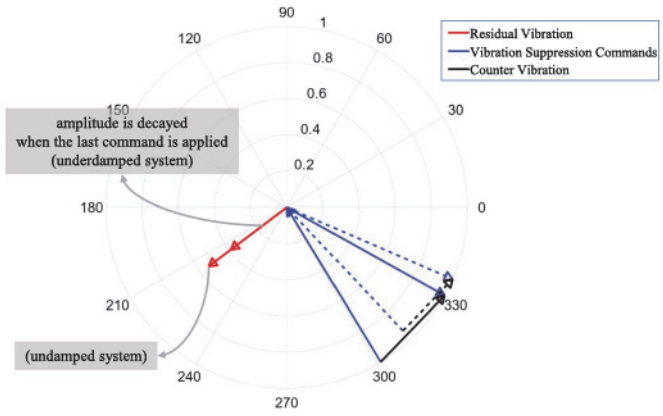

Fig. 7. Representation of residual vibrations in the complex plane. The solid lines represent an example for an undamped system. The dashed lines represent an example for an underdamped system.

suppression commands can be determined as follows:

$$\sum_{i=1}^{n} A_i \cdot e^{-\zeta\omega_n (t-t_i)} \cdot \cos\phi_i = 0 \tag{21}$$

$$\sum_{i=1}^{n} A_i \cdot e^{-\zeta\omega_n (t-t_i)} \cdot \sin\phi_i = 0. \tag{22}$$

The solutions satisfying both (21) and (22) are not unique due to nonlinearity in the equations. Schultz and Ueda have investigated on vibration suppression commands using a quantized system for point-to-point movements in [19]. Numerical approaches for searching a pattern of A and determining phases ϕ were used. Although one condition was relaxed that the system is undamped ($\zeta = 0$) in [19], it was concluded that no statements in regard to existence, nonexistence, or uniqueness of the solutions can be made using classical mathematical methods. Solutions to systems of nonlinear equations are still a topic of mathematics research.

In this study, commands after the tracking region are determined to suppress residual vibrations in a minimum command fashion. This introduces

$$\sum_{i=1}^{m_1+m_2} A_i = 1 \text{ such that } (m_1 + m_2) \text{ is minimized} \tag{23}$$

where m_1 and m_2 are the number of switching in tracking and vibration suppression commands, respectively.

If the last point of the tracking region is above the midpoint $\frac{\theta_{k+1}+\theta_k}{2}$, an additional even number of switches are required because $\sum_{i=1}^{m_1} A_i = 1$. Similarly, if the last point of the tracking region is below the midpoint $\frac{\theta_{k+1}+\theta_k}{2}$, an additional odd number of switches are required because $\sum_{i=1}^{m_1} A_i = 0$. In this case, one additional switch is not the minimum number that can satisfy (21) and (22), as B_{sum} is not necessarily an integer and decays in time. We include the first ON switch after the exposure window in the tracking commands to make $\sum_{i=1}^{m_1} A_i = 1$.

Let B_{track} and Φ_{track} be the amplitude and phase of the residual vibrations due to m_1 switches during the exposure window, respectively. Since B_{track} is approximately $[0, \frac{|A_i|}{2}]$, introducing two additional switches is sufficient to suppress the residual vibration. This can be explained by using the complex plane representation.

Fig. 7 shows the complex plane, and the red arrow represents the residual vibration due to tracking commands. The solid lines represent an example for an undamped system, and the dashed lines represent an example for an underdamped system. The residual vibration can

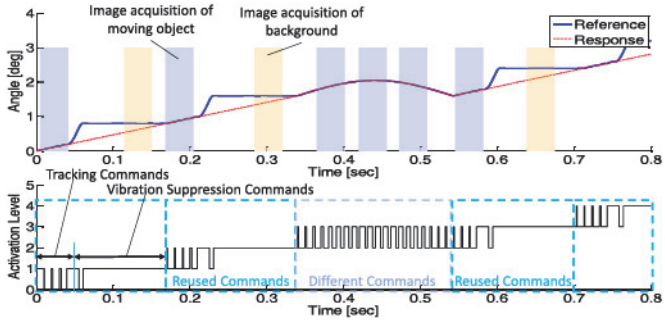

Fig. 8. Generated commands are resuable by suppressing residual vibrations in each increment if the velocity is constant. Also, both the object and background can be captured without motion blur in a short period of time by visual-motor coordination.

be suppressed in the next quadrant, where Φ_{track} exists. For vibration suppression, the sum of vectors in the complex plane must be equal to zero. A counter residual vibration whose amplitude and phase are B_{track} and $\pi + \Phi_{\text{track}}$, respectively, can be generated in the following quadrant by having two additional switches. The discrete switching commands for vibration suppression also satisfy (6) and (7).

The two additional phases ϕ_{vs1} and ϕ_{vs2} to suppress the residual vibration for an undamped system ($\zeta = 0$) can be given as

$$\phi_{vs1} = \Phi_{\text{track}} + \frac{\pi}{2} - \frac{\alpha}{2} \tag{24}$$

$$\phi_{vs2} = \phi_{vs1} + \alpha \tag{25}$$

where $\alpha = \text{acos}\left(1 - \frac{(B_{\text{track}})^2}{2}\right)$. Then, timing of the two commands, t_{vs1} and t_{vs2}, to suppress the residual vibration can be determined by using the following relationship:

$$t_i = \phi_i/\omega_n\,. \tag{26}$$

For an underdamped system, the amplitudes of the residual vibration and the first switch for vibration suppression are exponentially decaying, which introduces additional nonlinear terms compared to the undamped system. Due to this, the phases of each switch for an underdamped system exist slightly after that for an undamped system. The solutions to timing of the vibration suppression commands can be obtained by using numerical methods, and the phases of an undamped system can be used as a reference to find a local minimum.

The entire set of discrete switching commands for both tracking and vibration suppression can be summarized as

$$\mathbf{u}(t) = \sum_{i=1}^{m_1+2} A_i \cdot 1(t_i) \tag{27}$$

where $\boldsymbol{A} = [A_1 \cdots A_{m_1} \; -1 \; 1]$ and $\mathbf{t} = [t_1 \cdots t_{m_1} \; t_{vs1} \; t_{vs2}]$.

Fig. 8 shows one possible visual-motor application by suppressing residual vibrations after the exposure window. Tracking switching commands run first for object tracking, and vibration suppression switching commands follow for background image capturing. Repeating this switching in a short period of time enables updating images of both the object of interest and background. In addition, the generated commands in a single quantized increment are reusable if the velocity of the tracking profile is constant in multiple quantized increments. In addition, an arbitrary motion can be generated in the succeeding quantized region. This is because no residual vibrations exist when the tracking controller is initiated in each incremented position.

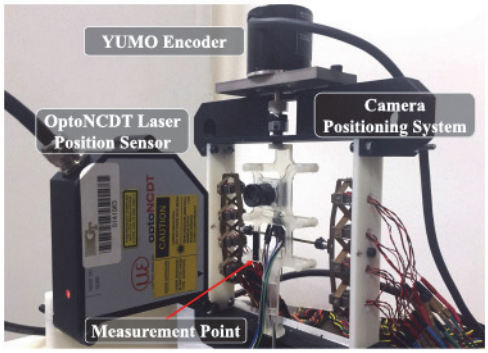

Fig. 9. Experimental setup for measuring the responses.

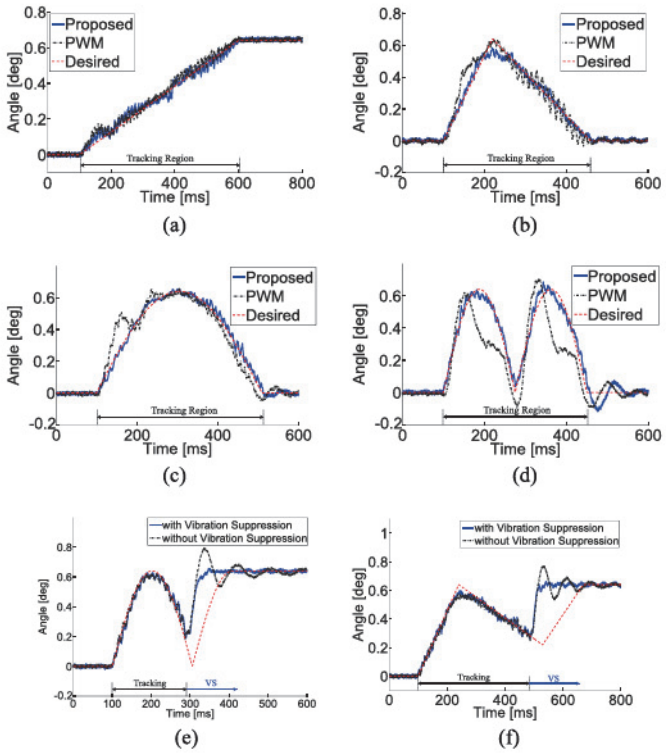

Fig. 10. Validation of the proposed controller. (a)–(d) Proposed method is directly compared with the reference and the PWM controller. (e) and (f) Comparisons between the proposed method, consisting of both the tracking and vibration suppression (VS) controllers, and the tracking-only controller. (a) Test #1: Tracking. (b) Test #2: Tracking. (c) Test #3: Tracking. (d) Test #4: Tracking. (e) Test #5: Tracking and VS. (f) Test #6: Tracking and VS.

V. Experimental Results and Discussions

A. Controller Validation by a Position Sensor

The proposed discrete controller for tracking an arbitrary velocity profile and vibration suppression is experimentally validated. The motion of the camera positioning system is directly compared with the reference motion. The experimental setup is shown in Fig. 9. The response is measured by a Micro-Epsilon optoNCDT 2200 laser position sensor. The position resolution, linearity, and measurement frequency of the laser sensor are 0.3 μm, 6 μm, and 10 kHz, respectively.

The robotic vision system was operated by a National Instruments cRIO-9024 running VxWorks at 1 kHz and cRIO-9118 running field-programmable gate arrays at 40 MHz. The robotic vision system employs a Ximea subminiature camera MU9PC-MH.

TABLE I
Test Conditions: Tracking Region

Test #	Mean Speed	ω_c	Test #	Mean Speed	ω_c
1	1.28 deg/sec	36.0 Hz	4	7.31 deg/sec	57.1 Hz
2	3.56 deg/sec	55.5 Hz	5	5.88 deg/sec	97.0 Hz
3	3.12 deg/sec	48.8 Hz	6	2.57 deg/sec	59.0 Hz

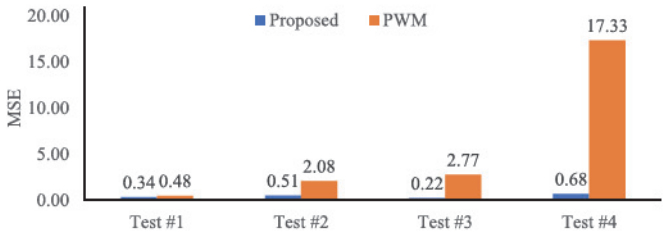

Fig. 11. MSE: Quantitative evaluation of the tracking performances.

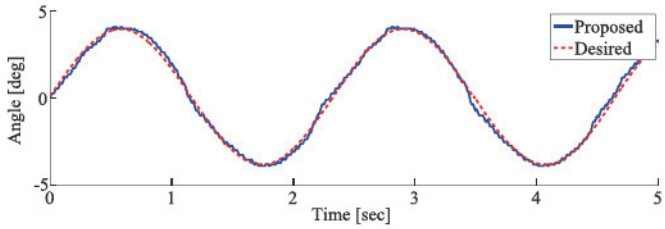

Fig. 12. Tracking a long motion profile with $\omega_c = 36$ Hz.

1) Tracking: Fig. 10(a)–(d) shows experimental comparisons of the tracking performance between the proposed controller and a conventional PWM method. For the PWM controller, the iterative linear–quadratic regulator method [20] was used, and the control law u was quantized to |u| at each sampling. A total of four different motion profiles were tested, where the speed ranged from 1.28 to 7.31 °/s, as described in Table I. All velocity profiles were in the range of a single PZT activation level. For a direct comparison, the PWM controller had the same amount of switching, and the commands were generated in an open-loop manner. The tracking commands were generated only in the indicated period. Thus, the response due to residual oscillations after the tracking region can be neglected in this experiment.

It can be observed from Fig. 10(a)–(d) that the proposed controller successfully tracked the slowly varying reference profiles with low control frequency ω_c and reduced switching. The proposed method outperformed the conventional PWM method. However, significant position errors are observed from the PWM method. Tracking performances are evaluated quantitatively by the average sum of squared error (MSE):

$$\text{MSE} = \frac{1}{2}\frac{\int_0^T \mathrm{e}^{\mathrm{T}} \cdot \mathrm{e} dt}{T} \tag{28}$$

where e is the position error.

Fig. 11 presents the integrated sum of tracking errors. It can be checked that the performance metric of the proposed method is better than that of the PWM method for all cases. This is because the PWM method does not account for dynamics of the system. Minor position errors are observed from the proposed method due to quantization effects and low control frequency; however, it was not significant.

Fig. 12 shows that the proposed controller is also capable of generating a long range of motion in a long period of time. The camera

TABLE II
RESULTS OF VIBRATION SUPPRESSION

Test #	Improvement in settling time	Reduction in switches
5	393 ms	16
6	239 ms	5

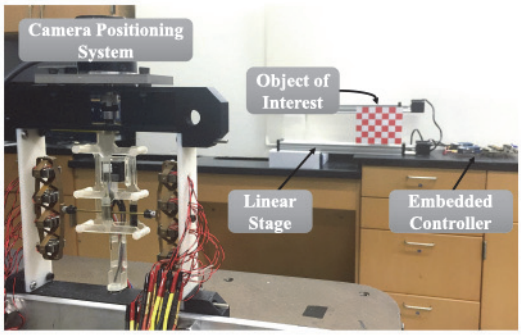

Fig. 13. Experimental setup for pseudotracking.

positioning system was controller at 36 Hz, and the response was measured by a YUMO E6B2-CWZ3E encoder due to limitation of the laser sensor.

2) Vibration Suppression: The vibration suppression commands after the tracking region discussed in Section IV-C were also validated using the same setup shown in Fig. 9. The proposed method consisting of both tracking and vibration suppression controllers was compared with the tracking-only controller. For the tracking-only controller, no further switches were generated after the image acquisition period.

It can be observed from Fig. 10(e) and (f) that the proposed controller successfully suppressed the residual vibration after the image acquisition period while reaching to the target discrete position. It improved the settling time and reduced the number of switchings, as demonstrated in Table II. Since the residual vibrations are completely suppressed, any desired motions can be generated in the succeeding quantized region using the same approach.

B. Controller Validation by Pseudotracking

For realization of smooth pursuit, in this study, the robotic positioning system tracks an object of interest and captures its image during the motion. The experimental setup for pseudotracking is shown in Fig. 13. A checkerboard was positioned by a linear stage, and the camera positioning system was pseudotracking the object at a constant velocity of 8 °/s. The proposed controller is capable of generating slower motion profiles than 8 °/s, as presented in the previous tests and demonstrated in Table I; however, the camera may capture a clean image of the interest object without tracking if the motion is substantially slow. It was assumed that motion of the object is known, since motion estimation of moving objects is not in the scope of this study.

The proposed controller generated discrete switching commands to match checkerboard motion during the exposure window. The obtained image would not exhibit blurriness, if the camera positioning system successfully tracks a moving object during the exposure window.

Two experiments were conducted, where VGA-size and UVGA-size images were obtained in the course of motion at 28.6 and 12.5 frames/s, respectively. Fig. 14 shows the cropped images of the obtained results. The first column shows the images obtained by the proposed method, and the last column shows the reference images obtained at rest. The

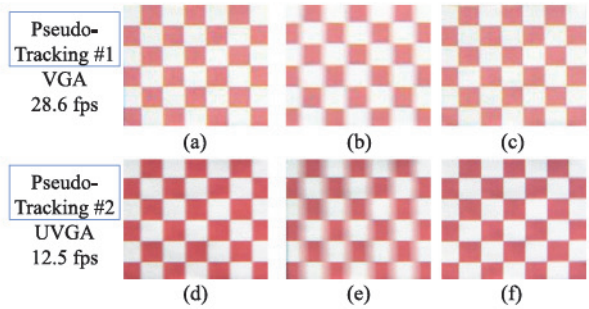

Fig. 14. Results of pseudotracking. (a) Tracking. (b) Camera at rest. (c) Reference. (d) Tracking. (e) Camera at rest. (f) Reference.

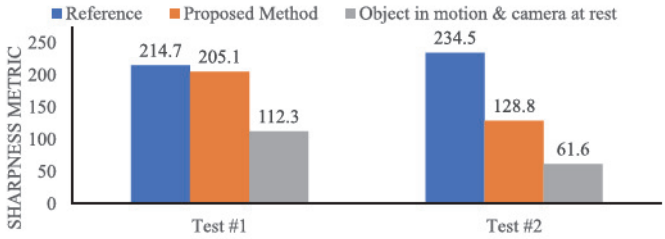

Fig. 15. Quantitative evaluations of the images obtained by pseudotracking.

images in the middle were obtained when the object was in motion, while the camera was at rest; the motion of the object is not negligible as they are blurry.

From tracking test #1, no significant blurriness was observed in the image obtained by the proposed method, as shown in Fig. 14(a). Thus, it can be concluded that the controller successfully matched the motion of the slowly moving object. From tracking test #2, the image obtained by the proposed method was comparable with the reference, as shown in Fig. 14(d); however, minor blurriness exists. This was mainly because the motion of the camera orientation system was rotational, while the motion of the object was translational. In addition, the degree of blurriness was amplified in test #2 due to a long exposure time. Although the camera positioning system successfully generated the desired movements, minor blurriness cannot be avoided.

The results are also evaluated in a quantitative manner. The performance metric is defined to calculate the sharpness of the edges on the checkerboard image as follows:

$$\text{Sharpness metric} = \frac{\sum_{k=1}^{h} \max(w(x) \cdot (\mathrm{I}_k(x) \otimes G_x))}{h} \tag{29}$$

where I_k is the kth horizontal line of the image, G_x is the horizontal Sobel kernel, w is a noise filter, $\otimes$ is the convolution operator, and h is the height of the image.

The quantitative evaluation is presented in Fig. 15. It can be observed that the images by the proposed method exhibit comparable sharpness with the reference. Although the value of the proposed method in test #2 is weaker than that of the reference image, this is due to a discrepancy in the motion vector and a long exposure time as aforementioned. The image obtained when the camera was at rest exhibits low values due to blurriness. We conclude that the proposed discrete switching controller was effective, since the sharpness of the images was preserved by tracking the object.

VI. Conclusion

This paper has presented a discrete switching controller to generate an arbitrary velocity profile for a quantized compliant actuator-driven robotic vision system. The proposed method is designed to match the velocity of the object of interest only during the exposure window. During the exposure window, tracking motion is generated by combining and optimizing a series of pulse-like commands at each primitive. Then, residual vibrations are suppressed, while reaching the desired quantized position. Although the classical feedback controller with PWM quantization is capable of generating an arbitrary velocity profile, it causes high-frequency switching that would damage the thin compliant mechanical structure. The proposed controller is an open-loop method and requires less frequent switching than the existing methods.

The proposed method was validated by comparisons with the reference and the PWM method and by pseudotracking the object. The experimental results show that the performance metrics of the proposed method were better than that of the conventional PWM method. In addition, after vibration suppression, the proposed method presented an improved settling time, while reaching to the desired discrete position.

References

[1] N. Barmack, "Modification of eye movements by instantaneous changes in the velocity of visual targets," *Vis. Res.*, vol. 10, no. 12, pp. 1431–1441, 1970.

[2] M. G. MacAvoy, J. P. Gottlieb, and C. J. Bruce, "Smooth-pursuit eye movement representation in the primate frontal eye field," *Cerebral Cortex*, vol. 1, no. 1, pp. 95–102, 1991.

[3] Y.-C. Lee, C.-C. Lan, C.-Y. Chu, C.-M. Lai, and Y.-J. Chen, "A pan–tilt orienting mechanism with parallel axes of flexural actuation," *IEEE/ASME Trans. Mechatronics*, vol. 18, no. 3, pp. 1100–1112, Jun. 2013.

[4] G. Cannata and M. Maggiali, "Models for the design of bioinspired robot eyes," *IEEE Trans. Robot.*, vol. 24, no. 1, pp. 27–44, Feb. 2008.

[5] T. Asfour, K. Welke, P. Azad, A. Ude, and R. Dillmann, "The Karlsruhe humanoid head," in *Proc. 8th IEEE-RAS Int. Conf. Humanoid Robots*, Dec. 2008, pp. 447–453.

[6] A. Ude, C. G. Atkeson, and G. Cheng, "Combining peripheral and foveal humanoid vision to detect, pursue, recognize and act," in *Proc. IEEE/RSJ Int. Conf. Intell. Robots Syst.*, Oct. 2003, vol. 3, pp. 2173–2178.

[7] A. Ude, T. Shibata, and C. G. Atkeson, "Real-time visual system for interaction with a humanoid robot," *Robot. Auton. Syst.*, vol. 37, no. 2, pp. 115–125, 2001.

[8] M. Bjorkman and D. Kragic, "Combination of foveal and peripheral vision for object recognition and pose estimation," in *Proc. IEEE Int. Conf. Robot. Automat.*, Apr. 2004, vol. 5, pp. 5135–5140.

[9] J. Turski, "Modeling active vision during smooth pursuit of a robotic eye," *Electron. Imag.*, vol. 2016, no. 10, pp. 1–8, 2016.

[10] J. D. Enderle and J. W. Wolfe, "Time-optimal control of saccadic eye movements," *IEEE Trans. Biomed. Eng.*, vol. BME-34, no. 1, pp. 43–55, Jan. 1987.

[11] S. S. Lehrer, "The regulatory switch of the muscle thin filament: Ca 2+ or myosin heads?" *J. Muscle Res. Cell Motility*, vol. 15, no. 3, pp. 232–236, 1994.

[12] J. Schultz and J. Ueda, "Nested piezoelectric cellular actuators for a biologically inspired camera positioning mechanism," *IEEE Trans. Robot.*, vol. 29, no. 5, pp. 1125–1138, Oct. 2013.

[13] M. D. Kim and J. Ueda, "Real-time panoramic image generation and motion deblurring by using dynamics-based robotic vision," *IEEE/ASME Trans. Mechatronics*, vol. 21, no. 3, pp. 1376–1387, Jun. 2016.

[14] M. D. Kim and J. Ueda, "Dynamics-based motion de-blurring for a PZT-driven, compliant camera orientation mechanism," *Int. J. Robot. Res.*, vol. 34, pp. 653–673, 2015.

[15] M. D. Kim and J. Ueda, "Dynamics-based motion deblurring improves the performance of optical character recognition during fast scanning of a robotic eye," *IEEE/ASME Trans. Mechatronics*, vol. 23, no. 1, pp. 491–495, Feb. 2018.

[16] M. D. Kim and J. Ueda, "Discrete switching commands for tracking and vibration suppression using a quantized, compliant camera orientation system," in *Proc. IEEE Int. Conf. Robot. Automat.*, May 2016, pp. 5177–5182.

[17] R. Jürgens, W. Becker, and H. Kornhuber, "Natural and drug-induced variations of velocity and duration of human saccadic eye movements: Evidence for a control of the neural pulse generator by local feedback," *Biol. Cybern.*, vol. 39, no. 2, pp. 87–96, 1981.

[18] S. C. Chapra and R. P. Canale, *Numerical Methods for Engineers*, vol. 2. New York, NY, USA: McGraw-Hill, 2012.

[19] J. Schultz and J. Ueda, "Experimental verification of discrete switching vibration suppression," *IEEE/ASME Trans. Mechatronics*, vol. 17, no. 2, pp. 298–308, Apr. 2012.

[20] W. Li and E. Todorov, "Iterative linear quadratic regulator design for nonlinear biological movement systems," in *Proc. 1st Int. Conf. Inform. Control, Automat. Robot.*, 2004, vol. 1, pp. 222–229.